Journal of Hazardous Materials 209–210 (2012) 137–145

Contents lists available at SciVerse ScienceDirect

Journal of Hazardous Materials

journal homepage: www.elsevier.com/locate/jhazmat

Efficient adsorption and visible-light photocatalytic degradation of tetracycline hydrochloride using mesoporous BiOI microspheres

Rong Hao[a], Xin Xiao[a,b], Xiaoxi Zuo[a], Junmin Nan[a,*], Weide Zhang[b,*]

[a] School of Chemistry and Environment, South China Normal University, Guangzhou 510006, PR China
[b] Nano Science Research Center, School of Chemistry and Chemical Engineering, South China University of Technology, Guangzhou 510640, PR China

ARTICLE INFO

Article history:
Received 10 September 2011
Received in revised form
24 November 2011
Accepted 1 January 2012
Available online 10 January 2012

Keywords:
Tetracycline hydrochloride
BiOI
Adsorption
Photocatalysis
Visible light

ABSTRACT

A novel microsphere-like BiOI hierarchical material was successfully synthesized by a one-step solution method at room temperature using polyvinylpyrrolidone (PVP) as structure directing reagent, its morphology, structure, surface area, photoabsorption were characterized, and the removal of tetracycline hydrochloride (TC) was evaluated under dark adsorption and visible light irradiation. It was shown that the BiOI microspheres formed in the precursor solution with PVP exhibit a mesoporous surface layer, 28.1 $m^2 g^{-1}$ surface area, 1.91 eV band gap energy (E_g value), and twofold removal ability to tetracycline hydrochloride (TC), i.e. adsorptive separation and visible light photocatalytic degradation. The adsorption process of TC on BiOI microspheres can be described by pseudo-second-order kinetics model and both Freundlich and Langmuir equations well described the adsorption isotherm but the former is better. More importantly, the BiOI microspheres exhibit an excellent photocatalytic degradation and mineralization capability to TC under visible light irradiation, which comes from its electronic band structure, high surface area and high surface-to-volume ratio. In addition, the BiOI microspheres are stable during the reaction and can be used repeatedly, showing promising prospect for the treatment of TCs in future industrial application.

© 2012 Elsevier B.V. All rights reserved.

1. Introduction

In the past decades, more and more residues of pharmaceuticals and personal care products (PPCPs) have been detected in the aquatic environment, and PPCPs are now recognized as a new class of pollutants and a subject arising public concern and scientific interest [1–3]. Thereinto, antibiotics were more frequently faced than other kinds of PPCPs due to their extensive use in human and veterinary medicine [4,5]. Especially for tetracyclines (TCs), the second most common antibiotics in both production and usage, have been widely used in human and animal treatment against infectious diseases, and their residues left in the environment can induce the development of antibiotic-resistant pathogens and cause serious problems for human health [6,7]. It is thus of great importance to develop efficient and cost-effective treatment technologies to remove these pollutants left in the aquatic environment.

In practice, the tetracyclines residues are hard to be treated by the traditional methods such as physical adsorption and biological degradation due to the difficult faced on the post-treatment of sorbents and the antibacterial nature of tetracyclines. As a promising method, the advanced oxidation processes (AOPs) have exhibited the predominance to remove the recalcitrant and non-biodegradable compounds due to their high efficiency in oxidizing a great variety of organic compounds through the generation of highly oxidizing hydroxyl radicals [8]. So far, the degradation of tetracyclines has been conducted by using Fenton reagent oxidation [9], ozonation [10,11] and photocatalytic oxidation [12–14] processes. And the photocatalytic technique is considered suitable for the degradation of TCs with high efficiency, high mineralization rate, simplicity of operation and low cost. However, the majority of photocatalytic processes are using nano TiO_2-based photocatalysts, and TiO_2 is effective only under ultraviolet irradiation ($\lambda < 380$ nm) because of its large band gap, which limits its practical application under solar light or indoor usage. What's more, the post-filtration procedures to separate photocatalysts and the gradual inactivity during the continuous using are also the defects of TiO_2-based nanomaterials to limit their application [15,16]. Therefore, it is helpful for the photocatalytic degradation of TCs to improve the properties of TiO_2-based photocatalysts, or to explore novel non-titania semiconductors with strong absorbance for broad ranged visible lights, high efficiency and relatively large particles for easily reuse.

As alternative photocatalysts, ternary oxide semiconductors, i.e. bismuth oxyhalides, have attracted considerable attention recently

* Corresponding authors. Tel.: +86 20 39310255; fax: +86 20 39310187.
E-mail address: jmnan@scnu.edu.cn (J. Nan).

0304-3894/$ – see front matter © 2012 Elsevier B.V. All rights reserved.
doi:10.1016/j.jhazmat.2012.01.006

owing to their unique layered-structure, which can induce the effective separation of photo-generated electron–hole pairs and achieve a high photocatalytic performance [17–19]. Among them, BiOI has the smallest band gap (~1.85 eV) and strong absorption in visible-light region. It has been reported that pollutants such as azo dyes [20–22] and phenolic compounds [23–25] can be effectively decomposed by BiOI-based photocatalysts under visible-light irradiation. In addition, the BiOI materials with high surface-to-volume ratio and anti-aggregation ability has also received growing concern [26–28] due to their potential reactivity and adsorption capability to the target pollutants [29–31]. However, until now, most of the synthesis of BiOI materials with three-dimensional (3D) or porous structures was carried out in complicated solvent systems under high temperature/pressure situations for long reaction period. It is essential to investigate simple, low energy and environment-friendly method to produce BiOI photocatalyst with controllable structure to meet the potential application in the treatment of TCs wastewaters. In our lab, a novel mesoporous BiOI microsphere visible-light photocatalyst was synthesized at room-temperature by a facile and easily scaled-up solution method through introducing structure directing reagent, i.e. Polyvinylpyrrolidone (PVP), in the reaction system. The as-synthesized BiOI microspheres exhibited high adsorption separation and visible-light photocatalytic degradation ability to TCs. In this paper, the synthesis and microstructure of mesoporous BiOI microspheres, and their adsorption and photocatalytic degradation of tetracycline hydrochloride (TC) are presented.

2. Experimental

2.1. Materials and preparation of BiOI microspheres

The tetracycline hydrochloride ($C_{22}H_{24}O_8N_2{\cdot}HCl$, Fig. S1 in Supplementary material) was purchased from Aladdin Reagent Co. Ltd. Bismuth nitrate pentahydrate ($Bi(NO_3)_3{\cdot}5H_2O$) and potassium iodide (KI) were bought from Tianjin Kermel Chemical Reagent Co. Ltd. Polyvinylpyrrolidone (PVP, the average molecular weight of PVP-K15, PVP-K30, and PVP-K90 is about 10,000, 58,000, and 130,000, respectively) was obtained from Shanghai Bio Life Science & Technology Co., Ltd. All chemicals were used as received without further purification. Distilled water was used to prepare solutions in the experiments.

In a typical synthesis of mesoporous BiOI microspheres, 0.728 g $Bi(NO_3)_3{\cdot}5H_2O$ and 0.249 g KI were firstly dissolved into 30 mL PVP solution, respectively. After that, KI solution was added dropwise into the $Bi(NO_3)_3$ solution under magnetic stirring condition, and then, the mixture was stirred at room temperature for 4 h. Afterwards, the precipitates were collected by centrifugation, washed several times with distilled water and ethanol, and dried in an oven overnight at 60 °C. For comparison, the random BiOI nanoplatelets were also synthesized using a similar process, except for without adding PVP to the reaction system.

2.2. Characterization of BiOI microspheres

The phase composition of the as-synthesized BiOI samples was identified by powder X-ray diffractometer (XRD, Y2000, Dandong, China) with Cu Kα as a radiation source. Fourier transform infrared spectrometer (FTIR) spectra were recorded on an IR Prestige-21 spectrometer (Shimadzu, Japan) by dispersing samples in KBr. Their morphology was characterized by scanning electron microscopy (SEM, JSM-6380-LA, JEOL, Japan). The specific surface area was measured by nitrogen adsorption–desorption isotherms at 77 K according to the Brunauer–Emmett–Teller analysis (BET, ASAP 2020, Micromeritics, USA). A desorption isotherm was used to determine the pore size distribution using the Barrett–Joyner–Halenda (BJH) method. The UV–vis diffuse refection spectra (DRS) were recorded on a UV–vis spectrophotometer (UV-3010, Hitachi, Japan) using $BaSO_4$ as a reference and were converted from reflection to absorbance by the Kubelka–Munk method.

The adsorption experiments were carried out in the dark surrounding at room temperature (25 ± 2 °C). In a typical adsorption experiment, 50 mL TC solution was poured into glass beaker (100 mL), and then 50 mg sample was added under constant magnetic stirring condition. Afterwards, 2.5 mL solution was timely taken out and the absorbent was removed from the solution using 0.45 μm cellulose acetate syringe membrane filter. The TC content in the filtration solution was measured on a UV–vis spectrophotometer (UV-1800, Shimadzu, Japan, λ = 357 nm).

The photocatalytic degradation experiments were carried out in a photochemical reactor (XPA-VII, Nanjing Xujiang Machine-electronic Plant, China), equipped with a 1000 W Xe lamp combined with a 420 nm cut-off filter as light source. All photocatalytic reactions were performed using the same initial conditions: 50 mL of TC solution (40 mg L^{-1}) was mixed with 50 mg catalyst, under constant magnetic stirring. Throughout the reaction, the concentration of TC in the solution was determined by a UV–vis spectroscopy (UV-1800, Shimadzu, Japan, λ = 357 nm) or analyzed by a high performance liquid chromatography (HPLC, LC-20AT, Shimadzu, Japan) using a C18 reverse phase column (5 μm, 4.6 mm × 250 mm) with Ultraviolet detector (λ = 357 nm). Methanol (HPLC-grade), acetonitrile (HPLC-grade) and 0.01 M oxalic acid buffer solution were used as mobile phase (8:20:72, v/v/v), respectively, at a flow rate of 1 mL min^{-1}. To identify the intermediates from the photocatalytic oxidation of TC, the liquid chromatography combined with mass spectrometry (LC–MS) equipped with an electrospray ionization source, which was operated in the negative ionization (PI) mode, were applied. The selective ion monitoring (SIR) mode with a dwell time of 200 ms was used to acquire the MS spectra of TC and its intermediates with a scan range of m/z 100–500. Total organic carbon (TOC) concentration was measured by automatic total organic carbon analyzer (TOC-V, Shimadzu, Japan).

3. Results and discussion

3.1. Characterization of BiOI microspheres

3.1.1. Surface morphology

As the SEM images shown in Fig. 1A, it was demonstrated that random BiOI nanoplatelets could be obtained when the reaction was performed without adding of PVP in the precursor solutions. Whereas, when the PVP with suitable content and molecular weight was added in the precursor solutions, microsphere-like BiOI materials could be synthesized (Fig. 1B–F). To investigate the influence of PVP on the formation of BiOI microspheres, a series of comparative experiments with different PVP contents (from 0.1 g to 1.0 g) and different PVP molecular weights (K15, K30 and K90) were carried out. Although the morphologies of these samples were all 3D microspheres, more regular microspheres with large surface area, designed morphology and better dispersion were obtained when PVP-K30 with a content of 0.2 g in $Bi(NO_3)_3$ and KI precursor solutions (shown as Fig. 1B). In addition, in our other experiment, it was shown that this sample, which will be investigated in the following experiments, also exhibited higher photocatalytic performances.

The observation in Fig. 1A suggests the main morphology of the contrast sample is 2D nanoplatelets with an average thickness of ~50 nm and uneven size. From the low-magnification SEM image of Fig. 1B, one can see that the sample consists of a large quantity of

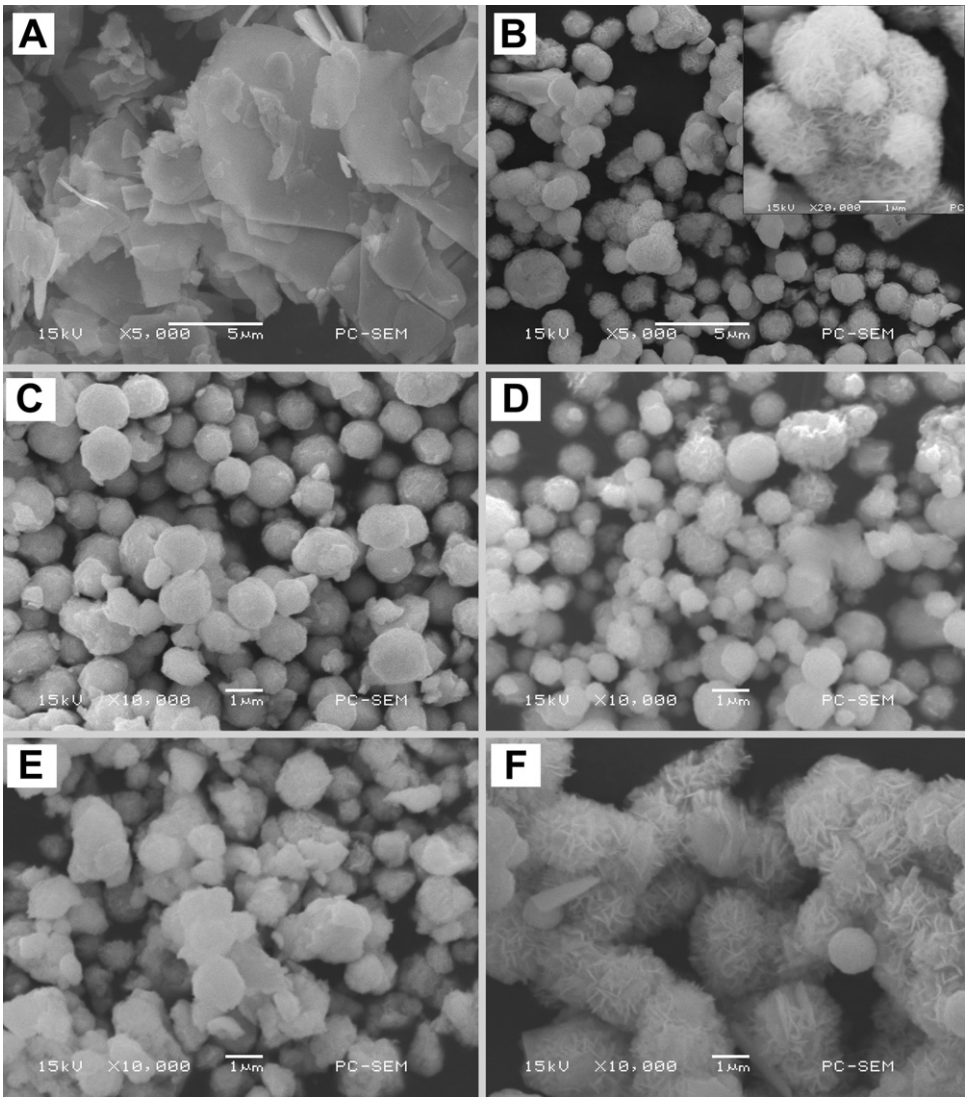

Fig. 1. SEM images of (A) random BiOI nanoplatelets, and (B–F) BiOI microspheres synthesized in adding of 0.2 g PVP-K30 (inset: higher-magnification SEM image), 0.1 g PVP-K30, 1.0 g PVP-K30, 0.2 g PVP-K15, and 0.2 g PVP-K90, respectively.

microspheres with diameters ranging from 1.5 to 3 μm. The higher magnification SEM image (inset of Fig. 1B) exhibits the detailed morphology of the microspheres-like nanostructure of the sample, which reveals that the entire structure of the architecture is built from several dozen nanolamellas. These nanolamellas are ~15 nm thick, and connected to each other to form 3D structures.

It is reasonably assumed that PVP plays the key role in the formation of such 3D spherical architectures. As is well known, BiOI has a layered structure characterized by $[Bi_2O_2]$ slabs interleaved by double slabs of I atoms, which results in the formation of platelet morphology (see Fig. 1A) [19,29,30]. However, in the presence of PVP polymer surfactant, the PVP may act as a potential crystal face inhibitor in the system, which benefits the formation of oriented nucleation, leading to the construction of anisotropic growth of the nanosheets. What's more, the PVP can also play a stabilizer to adsorb on the surfaces of BiOI nanosheets by coordinating with both nitrogen and oxygen atoms in the polar pyrrolidone groups, which may exhibit steric hindrance and prompt the formation of 3D spherical architectures from individual nanosheets due to the cross-linking ability of PVP with the long chain structure and multiple coordinating sites [32–35]. The main process is schematically illustrated in Fig. 2.

3.1.2. BET surface areas and pore structure

The specific surface area and porosity of the as-synthesized samples were investigated by using nitrogen adsorption and desorption isotherms. As shown in Fig. 3, the isotherm of BiOI microspheres is identified as type IV with a H3 hysteresis loop, which suggests its mesoporous feature [35,36]. The specific surface area of the sample was calculated from N_2 isotherms and was found to be as much as 28.1 $m^2 g^{-1}$. And the corresponding pore size distribution of BiOI microspheres confirms that it contains smaller mesopores about 3.5 nm diameter and larger pores centered at 6.3 nm diameter in a broad distribution, determined by using the BJH method (inset of Fig. 3). The small pores presumably arise from the nanosheets, whereas the large pores may be attributed to the internanosheet spaces [37]. However, the contrast sample (randomly aggregated nanoplatelets) almost had no hysteresis loop and the pore size distribution curve is turned into a line, indicating the small surface area and disappearance of pores. The BET surface area of the BiOI nanoplatelets was calculated to be 5.5 $m^2 g^{-1}$, which is less than one-fifth of the BiOI microspheres. It is well-known that porous solids have excellent adsorptive properties that possess numerous applications in catalysis and separation. Therefore, the as-synthesized BiOI microspheres sample is reasonable to expect

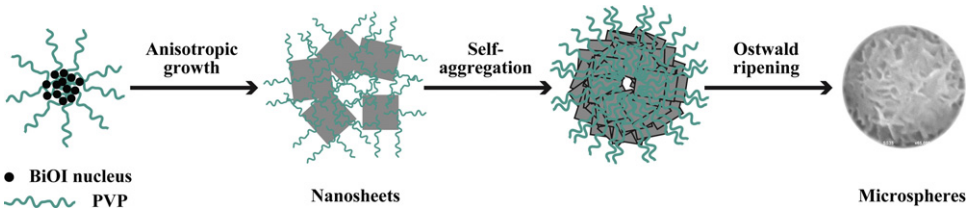

Fig. 2. Schematic illustration of the growth process of mesoporous BiOI microspheres.

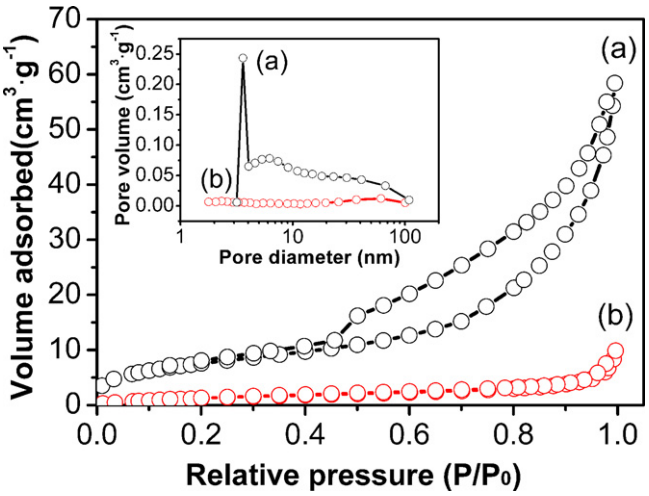

Fig. 3. Nitrogen adsorption–desorption isotherms and the corresponding pore size distributions curve (inset) of (a) BiOI microspheres and (b) BiOI nanoplatelets.

that it has a priority to exert its excellent adsorption and photocatalytic activity.

3.1.3. Crystal structure

The powder X-ray diffraction (XRD) pattern provides crystal structure and phase information of the as-synthesized samples. Fig. 4 shows the XRD patterns of the as-synthesized mesoporous BiOI microspheres and random BiOI nanoplatelets. All of the diffraction peaks can be clearly indexed as the tetragonal phase of BiOI (JCPDS No. 73-2062). No impurity peaks are observed, indicating a high purity of the products. However, the diffraction peaks of mesoporous BiOI microspheres are broader with lower intensity than that of BiOI nanoplatelets, indicating its smaller particle size [38]. The average size of crystallites can estimate based on the broadening of corresponding X-ray diffraction peaks by using Scherer formula [39]:

$$D = \frac{K\lambda}{\beta \cos\theta} \quad (1)$$

where λ is the wavelength of the X-ray radiation ($\lambda = 0.15418$ nm), K is the Scherer constant ($K = 0.9$), θ is the X-ray diffraction angle, and β is the full-width at half-maximum (FWHM) of the (0 1 2) plane after subtracting the instrumental broadening. Then the crystal size of the mesoporous BiOI and the nanoplatelets were estimated to be about 15 nm and 37 nm, respectively, which is in good agreement with the earlier SEM observed. In addition, the relative intensity of the {0 0 1} peaks in BiOI microspheres are obviously much lower than that of random nanoplatelets, indicating that the crystal structure of BiOI is anisotropically grown in the presence of PVP.

In order to examine the influence of drying temperature on crystallization and composition of the products, a sample was synthesized using same process of BiOI microspheres but drying under room temperature and then analyzed by XRD as well as compared with the sample that drying at 60 °C. As shown in Fig. S2 (Supplementary material), there are no obvious differences in structure and crystallization between these two cases, which imply that the BiOI synthesized by this method under room temperature is well crystallization. With the view of assessing any residual PVP in the BiOI microspheres, FTIR investigation was carried out, as shown in Fig. S3 (Supplementary material), which found that that on the final products no residual PVP was detected [40]. It indicates that the washing procedure was effective in the removal of the PVP from the sample in current situation.

3.1.4. Photoabsorption property

The energy band structure feature of a semiconductor is considered as a key factor to determinate its photocatalytic activity [41]. Fig. 5 shows the UV–vis absorption spectra of the as-synthesized BiOI microspheres and random platelets. The both samples exhibit strong photoabsorption from ultraviolet to visible light but the

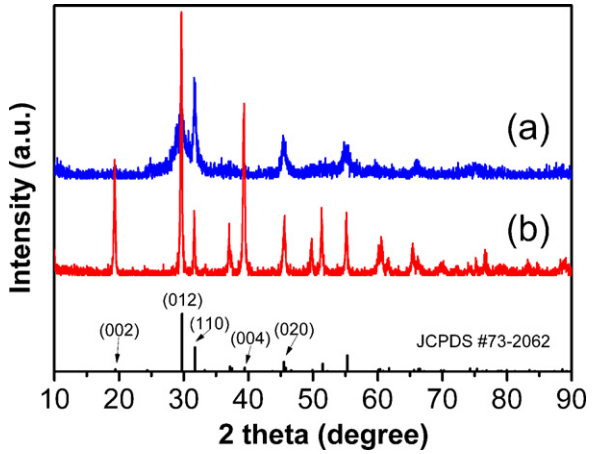

Fig. 4. XRD patterns of (a) mesoporous BiOI microspheres and (b) random BiOI nanoplatelets.

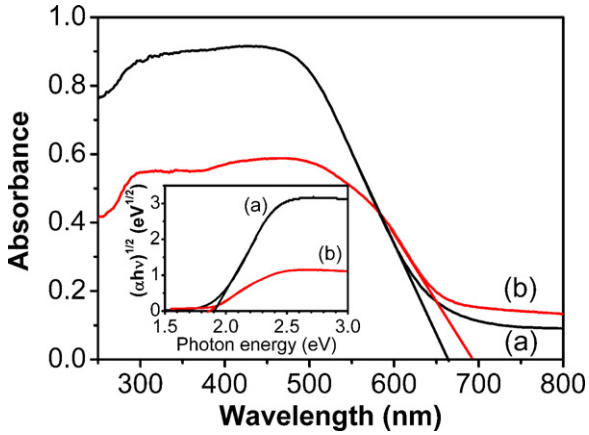

Fig. 5. UV–vis diffuse reflectance spectra of (a) BiOI microspheres and (b) random nanoplatelets. The inset shows the plots of $(\alpha h\nu)^{1/2}$ vs. photon energy ($h\nu$).

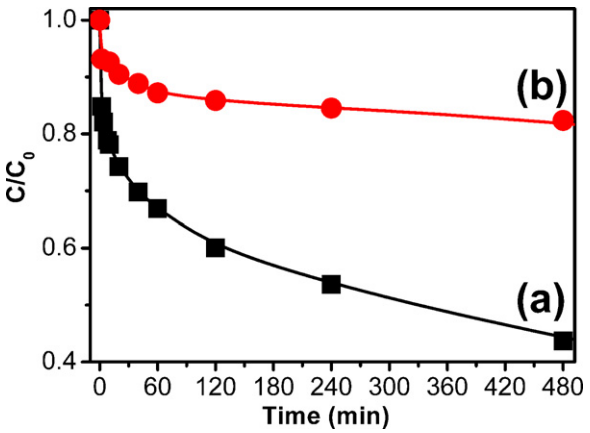

Fig. 6. Adsorption kinetics curves of TC (initial concentration 40 mg L^{-1}) on (a) BiOI microspheres and (b) BiOI nanoplatelets.

microspheres is better absorption, and from which the optical absorption edges are 663 nm and 692 nm, respectively. The band gap (E_g) of the samples can be evaluated from the following equation [19]:

$$\alpha(h\nu) = A(h\nu - E_g)^{n/2} \quad (2)$$

where α, ν, E_g, and A are the absorption coefficient, light frequency, band gap energy, and a constant, respectively. Among them, n depends on the characteristics of the transition in a semiconductor. For BiOX, the value of n is 4 for the indirect transition. For the diffused reflectance spectra, the Kubelka–Munk function can be used instead of α for estimating the optical absorption edge energy [42]. Then the band gap energies (E_g) of BiOI can be thus estimated from a plot of $(\alpha h\nu)^{1/2}$ versus photon energy ($h\nu$), as shown in the inset of Fig. 5. The intercept of the tangent to the x-axis will give a good approximation of the band gap energy for the BiOI powders. The estimated band gap energies of the samples are calculated to be about 1.91 eV for BiOI microspheres and 1.86 eV for BiOI platelets. The values determined in this work are in good agreement with those reported in literatures [43–46].

3.2. Sorption kinetics and isotherms of BiOI microspheres

3.2.1. Adsorption kinetics

The adsorption is one of the effective physical processes for the removal of TCs from the wastewater [47–50]. In addition, as mentioned above, the as-synthesized BiOI microspheres exhibit 3D mesoporous structure and a larger specific surface area, thus, the sorption behavior of TC on the BiOI microspheres was evaluated. The sorption behaviors of TC molecules on BiOI microspheres and random nanoplatelets are shown in Fig. 6. In comparison with the nanoplatelets, the BiOI microspheres exhibit excellent adsorption capacity: about 56% of TC in the solution with the initial concentration of 40 mg L^{-1} was adsorbed within 6 h, while only 17.6% of TC was removed by BiOI platelets during the same period. The enhancement of adsorption capacity is attributed to the unique structure feature and large BET surface area of 3D BiOI microspheres due to the adding of PVP as surfactant and structure directing reagent in the reaction system.

The adsorption of TC on BiOI microspheres in the solutions with difference initial concentrations was evaluated, as shown in Fig. 7A. The pseudo-second-order kinetics model, which assumes that the sorption rate is controlled by chemical sorption and the sorption capacity is proportional to the number of active sites on the

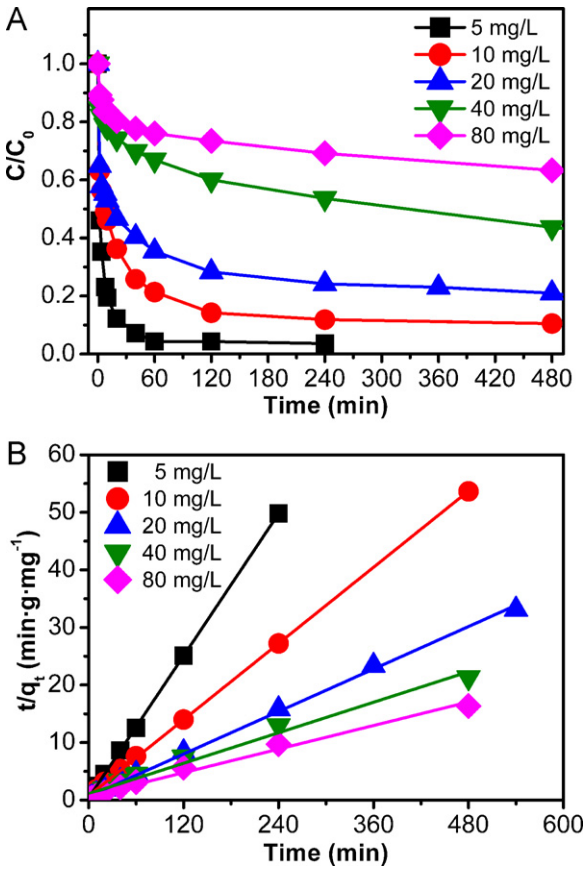

Fig. 7. (A) Adsorption of TC with different initial concentrations using 50 mg BiOI microspheres; and (B) Plots of TC adsorption on BiOI microspheres fitted by pseudo-second-order kinetics model.

adsorbent [27,51,52], was used to fit the kinetics data. The pseudo-second-order model can be expressed in the form as follows:

$$\frac{t}{q_t} = \frac{t}{q_e} + \frac{1}{kq_e^2} \quad (3)$$

where t, q_t, q_e and k (or k_{app}) are the adsorption time, adsorption capacity for a specific time, equilibrium adsorption capacity, and pseudo-second-order apparent rate constant, respectively. q_e and k can be obtained from the slope and intercept of the linear plot of t/q_t versus t (see Fig. 7B). The fitted parameters and the calculated data are given in Table 1. The results with good correlation coefficients ($R^2 > 0.99$) for the pseudo-second-order kinetic model imply the interaction of chemical adsorption could possibly occur during the adsorption process.

3.2.2. Adsorption isotherms

The Langmuir and Freundlich isotherm models were selected to evaluate the adsorption capacity of BiOI microspheres and understand the interactions between adsorbate and adsorbent, which

Table 1
Adsorption kinetics parameters of TC on BiOI microspheres at 298 K with the pseudo-second-order model.

C_0 (mg L^{-1})	$k_{app} \times 10^2$ (g mg^{-1} min^{-1})	R^2	q_e (mg g^{-1})	C_e (mg L^{-1})
5	11.10	0.9999	4.8604	0.1396
10	1.67	0.9992	9.0605	0.9395
20	0.60	0.9990	16.2504	3.7496
40	0.18	0.9925	22.6427	17.3573
80	0.13	0.9903	29.3100	50.6900

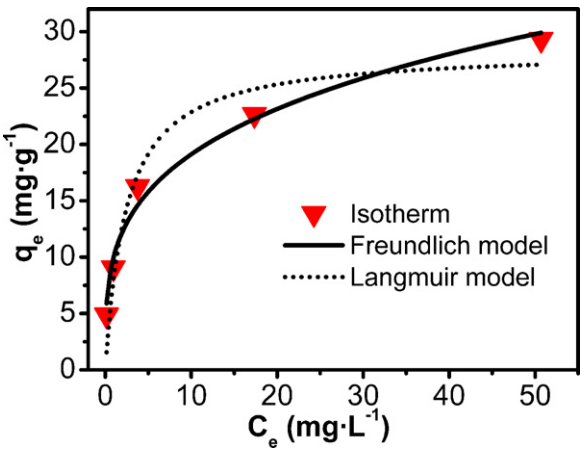

Fig. 8. Adsorption isotherm for TC on BiOI microspheres modeled by using Langmuir model and Freundlich model, respectively.

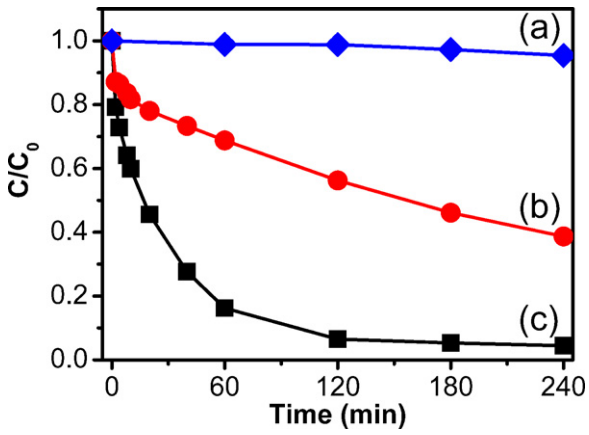

Fig. 9. Degradation of TC in the solution with initial concentration of 40 mg L^{-1} under visible-light irradiation on (a) Blank (without catalyst), (b) BiOI platelets, and (c) BiOI microspheres, respectively.

assumes that the sorption occurred at the specific homogeneous sites or heterogeneous surface within the adsorbent [51,53]. These two models can be expressed respectively as:

$$q_e = q_m \frac{bC_e}{1 + bC_e} \quad (4)$$

$$q_e = K_F C_e^n \quad (5)$$

where q_e, q_m, C_e, and b are the equilibrium concentration, the theoretical monolayer capacity, the liquid equilibrium concentration of adsorbate ($q_e = (C_0 - C_e) \times V/m$) and adsorption equilibrium constant, whereas K_F and n are the Freundlich constants representing the adsorption capacity and linearity index (departures of n from 1 imply nonlinear adsorption), respectively. The results modeled using the two isotherm models were shown in Fig. 8, and the data from the fitted results are presented in Table 2.

The fitting curves and correlation coefficient values both indicate the equilibrium sorption data are satisfactorily fitted with Freundlich and Langmuir models, and Freundlich model yields

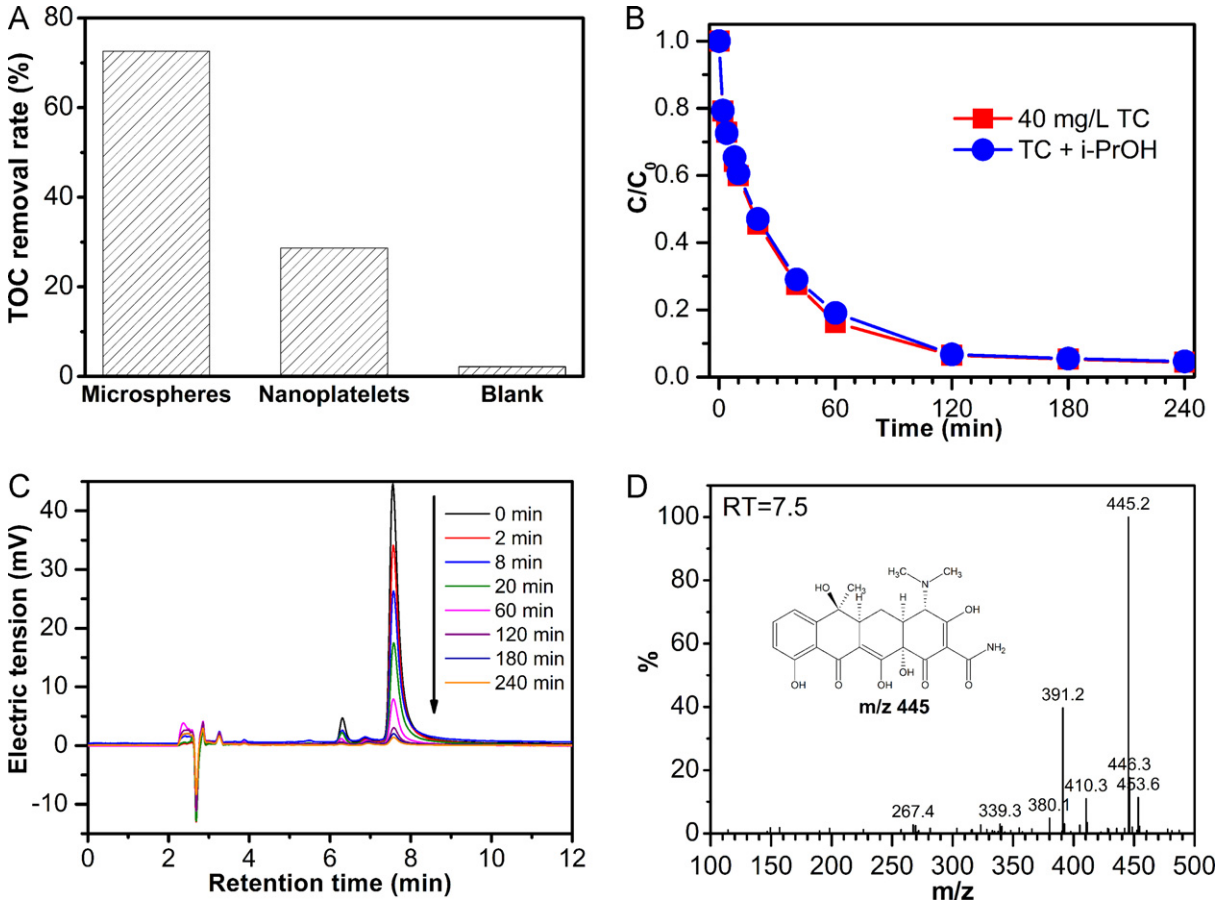

Fig. 10. (A) TOC removal ratio of TC (C_0 = 40 mg L^{-1}) over the BiOI microspheres, BiOI platelet and directly photolysis under visible light irradiation for 4 h; (B) Photocatalytic degradation of TC over BiOI microspheres in the absence and presence of *i*-PrOH; (C) HPLC chromatograms of TC solutions over the BiOI microspheres for different photocatalytic reaction times; and (D) Mass spectra and corresponding proposed structures at retention time = 7.5 min.

Table 2
Langmuir and Freundlich isotherm constants for TC adsorption on BiOI microspheres at 298 K.

Langmuir model			Freundlich model		
q_m (mg g^{-1})	b (L mg^{-1})	R^2	K_F (mg$^{1-1/n}$ L$^{1/n}$ g^{-1})	n	R^2
28.35456	0.41656	0.9209	10.14203	0.27539	0.98255

a somewhat better fit than that of Langmuir model. This indicates that the effect of surface heterogeneity is more pronounced [48,54,55], in other word, a stronger adsorbate–adsorbent interaction is formed, which is also in good agreement with the earlier investigation on adsorption kinetics.

3.3. Photocatalytic properties of BiOI microspheres

3.3.1. Comparison of photocatalytic activities of BiOI samples

The photocatalytic degradation of TC in the presence of as-synthesized BiOI samples was investigated and shown in Fig. 9. It is clearly indicated that the TC could hardly be degraded without any photocatalyst (Blank) while the BiOI microspheres shows much higher activity than that of the BiOI nanoplatelets with identical visible light exposure. After irradiation for 120 min, only 44% TC removal over the nanoplatelets is observed, while the removal ratio on the microspheres reaches 94%, and for comparison, about 40% of TC adsorbed on BiOI microspheres under the dark during the same period (see Fig. 6).

Several reasons may account for the higher photocatalytic activity of the BiOI spherical architectures synthesized by the as-proposed method as compared to the randomly aggregated nanoplatelets. Firstly, the photocatalytic process is closely related to the adsorption of reactant molecules on the surface of the catalyst. As mentioned above, the surface area of the microspheres is more than 5 times to that of the nanoplatelets. As a result, more coordination sites on the unsaturated surface are exposed to the solution and more efficient transport for the reactant molecules to access the active sites hence enhances the photocatalytic efficiency [19,29]. In order to rule out the effect of surface areas of the photocatalysts on their photocatalytic activities, we normalized the photocatalytic degradation rates (fitted by pseudo-first-order kinetics) by the surface areas [20] and found that the degradation rate of BiOI microspheres (7.06×10^{-4} g min^{-1} m^{-2}) is actually even slightly lower than that of randomly aggregated nanoplatelets (7.24×10^{-4} g min^{-1} m^{-2}). Therefore, it can conclude that the enhanced photocatalytic activity of microsphere-like BiOI is mainly attributed to its high surface area. Secondly, the high surface-to-volume ratios of microspheres are in favor of the transfer of electrons and holes to the surface and facilitate the degradation of TC. In addition, the high catalytic activity is also related to the hierarchical structure, such 3D interconnected channels formed by BiOI nanolamellas provide efficient transport paths for reactants and products in photocatalytic reactions.

3.3.2. Evaluation of the mineralization of TC

The concentration of total organic carbon (TOC) was chosen as a mineralization index of the degradation of TC. After photocatalytic reaction for 4 h using the as-synthesized BiOI microspheres and BiOI nanoplatelet or directly photolysis under visible light irradiation, the mineralization of TC were monitored through TOC analyzer, and the results are shown in Fig. 10A. It can be seen that when the process is not involved in any catalyst (Blank), only 2.16% TOC was removed, while 28.68% or 72.58% TOC were removed using the BiOI nanoplatelet or BiOI microspheres for 4 h, respectively. According to literature previously [56], the holes photogenerated on the surface of BiOI could not react with OH^-/H_2O to form •OH

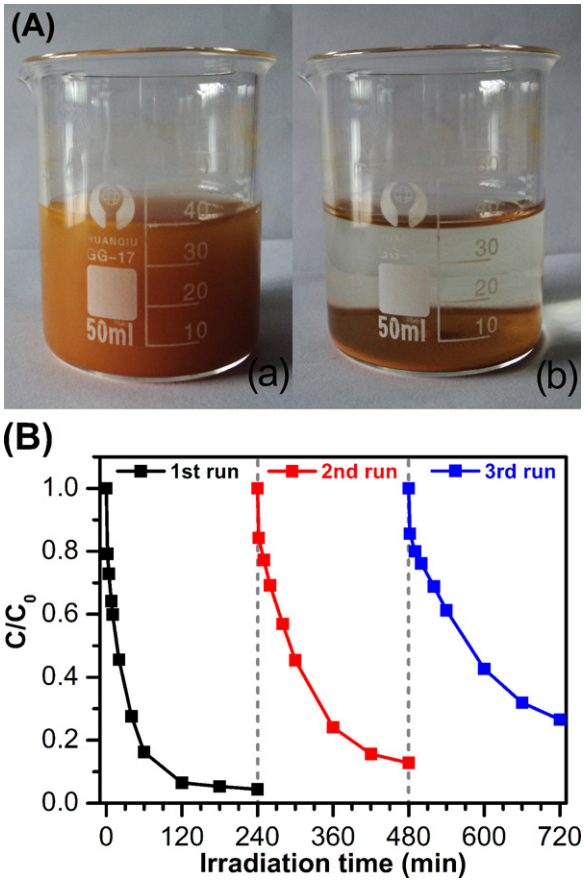

Fig. 11. (A) Experiments of natural settlement: (a) settled naturally after 30 min and (b) BiOI powder suspended in TC solutions; (B) Recycling properties of BiOI microsphere photocatalyst.

under visible light due to the standard redox potential of Bi^{5+}/Bi^{3+} (E^0 = 1.59 V at pH 0) is smaller than that of •HO/OH^- (1.99 V). However, the valence band edge potential (E_{VB}) of BiOI is ~2.42 V, which implies that it may have higher oxidative activity than that of •OH. A supplementary experiment was carried out through adding isopropanol (*i*-PrOH, used as the •OH quencher) to the photoreaction system, as shown in Fig. 10B, which suggested that TC photodegradation by BiOI is dominated by direct holes oxidation rather than oxidized by •OH. More importantly, the TOC removal efficiency on BiOI microspheres in current study is enhanced when compared with available literature data [10,57,58], especially for the results achieved by visible light photocatalytic processes. Fig. 10C illustrates the HPLC chromatograms of TC solution at varied reaction times. It can be seen from Fig. 10C that TC eluted at retention time of 7.5 min rapidly disappeared with the increasing of reaction time, which is also in agreement with the observation in UV–vis spectra. Then LC–MS technology was used to analyze the reaction intermediates during the photocatalytic process, as displayed in Fig. 10D. The result shows that only tetracycline ion ($[M+H]^+$) was detected [59] under current experimental conditions. Consequently, it can be safely concluded that TC can be effectively mineralized by the as-synthesized BiOI microspheres under visible light irradiation.

3.3.3. Recycle of BiOI microspheres

It is well known that the photocatalysts with small size present a superior activity due to the small crystal size allows more efficient transfer of electron–holes generated inside the crystal to the surface. However, in a particular photocatalytic process, the separation of these small particles from suspended solution after reaction could be very difficult for the recycle use. Due to the relative larger

size, the photocatalyst of BiOI microspheres have taken an advantage over other nanostructure catalysts for separating catalysts by a simple filtration step or even a natural sedimentation (see Fig. 11A).

To investigate the recyclability of the BiOI microspheres, sample powders after photocatalytic reactions were collected by natural settling and reused in the photocatalytic reaction for 3 times under the same conditions. As shown in Fig. 11B, the BiOI sample displays a good stability and maintains a high photocatalytic performance during three reaction cycles. The photocatalytic performance of sample decreased gradually may be due to the mass loss during the sedimentation and transferring processes and the gradually decline in adsorptive capacity of the catalyst. The results indicate that the mesoporous BiOI microspheres prepared by this facile method are stable for the photocatalysis of pollutant molecules, which is important for its practical application.

4. Conclusions

In summary, mesoporous BiOI microspheres have been successfully synthesized by a facile solution method at room temperature using PVP as surfactant and structure directing reagent. SEM observation shows that the microspheres-like hierarchical structure of the sample is built from several dozen nanolamellas connected to each other, and BET analysis reveals that the sample has a large specific surface area with mesoporous feature. As expected, the mesoporous BiOI microspheres exhibit a good capability for the adsorptive separation and an excellent visible-light induce photocatalytic in degradation of TC, which is ascribed to their high BET surface area, energy band structure and high surface-to-volume ratios. What is more, the as-synthesized mesoporous BiOI microspheres shown a high mineralization ratio of TC and can easily separated for recycling use, which indicates it is a very promising prospect for the treatment of TCs in industrial application.

Acknowledgements

This study was financially supported by the Natural Science Funds of Department of Education (Grant no. 05Z008) and the Science and Technology Projects (Grant no. 2007B030101007) of Guangdong Province.

Appendix A. Supplementary data

Supplementary data associated with this article can be found, in the online version, at doi:10.1016/j.jhazmat.2012.01.006.

References

[1] C.G. Daughton, T.A. Ternes, Pharmaceuticals and personal care products in the environment: agents of subtle change? Environ. Health Perspect. 107 (1999) 907–938.
[2] T.A. Ternes, A. Joss, H. Siegrist, Peer reviewed: scrutinizing pharmaceuticals and personal care products in wastewater treatment, Environ. Sci. Technol. 38 (2004) 392–399.
[3] J.B. Ellis, Pharmaceutical and personal care products (PPCPs) in urban receiving waters, Environ. Pollut. 144 (2006) 184–189.
[4] S. Thiele Bruhn, Pharmaceutical antibiotic compounds in soils – a review, J. Plant Nutr. Soil Sci. 166 (2003) 145–167.
[5] A.K. Sarmah, M.T. Meyer, A. Boxall, A global perspective on the use, sales, exposure pathways, occurrence, fate and effects of veterinary antibiotics (VAs) in the environment, Chemosphere 65 (2006) 725–759.
[6] L.L. Ji, Y.Q. Wan, S.R. Zheng, D.Q. Zhu, Adsorption of tetracycline and sulfamethoxazole on crop residue derived ashes: implication for the relative importance of black carbon to soil sorption, Environ. Sci. Technol. 45 (2011) 5580–5586.
[7] N. Pastor-Navarro, A. Maquieira, R. Puchades, Review on immunoanalytical determination of tetracycline and sulfonamide residues in edible products, Anal. Bioanal. Chem. 395 (2009) 907–920.
[8] J. Jeong, W.H. Song, W.J. Cooper, J. Jung, J. Greaves, Degradation of tetracycline antibiotics: mechanisms and kinetic studies for advanced oxidation/reduction processes, Chemosphere 78 (2010) 533–540.
[9] I.R. Bautitz, R. Nogueira, Degradation of tetracycline by photo-Fenton process – solar irradiation and matrix effects, J. Photochem. Photobiol. A 187 (2007) 33–39.
[10] M.H. Khan, H. Bae, J.Y. Jung, Tetracycline degradation by ozonation in the aqueous phase: proposed degradation intermediates and pathway, J. Hazard. Mater. 181 (2010) 659–665.
[11] M.C. Dodd, H. Kohler, U. Von Gunten, Oxidation of antibacterial compounds by ozone and hydroxyl radical: elimination of biological activity during aqueous ozonation processes, Environ. Sci. Technol. 43 (2009) 2498–2504.
[12] C. Reyes, J. Fernández, J. Freer, M.A. Mondaca, C. Zaror, S. Malato, H.D. Mansilla, Degradation and inactivation of tetracycline by TiO_2 photocatalysis, J. Photochem. Photobiol. A 184 (2006) 141–146.
[13] C. Zhao, H. Deng, Y. Li, Z. Liu, Photodegradation of oxytetracycline in aqueous by 5A and 13X loaded with TiO_2 under UV irradiation, J. Hazard. Mater. 176 (2010) 884–892.
[14] R.A. Palominos, M.A. Mondaca, A. Giraldo, G. Pe Uela, M. Pérez-Moya, H.D. Mansilla, Photocatalytic oxidation of the antibiotic tetracycline on TiO_2 and ZnO suspensions, Catal. Today 144 (2009) 100–105.
[15] M. Anpo, M. Takeuchi, The design and development of highly reactive titanium oxide photocatalysts operating under visible light irradiation, J. Catal. 216 (2003) 505–516.
[16] D. Chatterjee, S. Dasgupta, Visible light induced photocatalytic degradation of organic pollutants, J. Photochem. Photobiol. C 6 (2005) 186–205.
[17] X.F. Chang, J. Huang, C. Cheng, Q. Sui, W. Sha, G.B. Ji, S.B. Deng, G. Yu, BiOX (X = Cl, Br, I) photocatalysts prepared using $NaBiO_3$ as the Bi source: Characterization and catalytic performance, Catal. Commun. 11 (2010) 460–464.
[18] Z.T. Deng, D. Chen, B. Peng, F.Q. Tang, From bulk metal Bi to two-dimensional well-crystallized BiOX (X = Cl, Br) micro- and nanostructures: synthesis and characterization, Cryst. Growth Des. 8 (2008) 2995–3003.
[19] X. Zhang, Z.H. Ai, F.L. Jia, L.Z. Zhang, Generalized one-pot synthesis, characterization, and photocatalytic activity of hierarchical BiOX (X = Cl, Br, I) nanoplate microspheres, J. Phys. Chem. C 112 (2008) 747–753.
[20] Y. Wang, K. Deng, L. Zhang, Visible light photocatalysis of BiOI and its photocatalytic activity enhancement by in situ ionic liquid modification, J. Phys. Chem. C 115 (2011) 14300–14308.
[21] C. Yu, J.C. Yu, C. Fan, H. Wen, S. Hu, Synthesis and characterization of Pt/BiOI nanoplate catalyst with enhanced activity under visible light irradiation, Mater. Sci. Eng. B 166 (2010) 213–219.
[22] X. Zhang, L. Zhang, T. Xie, D. Wang, Low-temperature synthesis and high visible-light-induced photocatalytic activity of BiOI/TiO_2 heterostructures, J. Phys. Chem. C 113 (2009) 7371–7378.
[23] Y. Li, J. Wang, H. Yao, L. Dang, Z. Li, Chemical etching preparation of BiOI/Bi_2O_3 heterostructures with enhanced photocatalytic activities, Catal. Commun. 12 (2010) 660–664.
[24] Y. Li, J. Wang, H. Yao, L. Dang, Z. Li, Efficient decomposition of organic compounds and reaction mechanism with BiOI photocatalyst under visible light irradiation, J. Mol. Catal. A-Chem. 334 (2010) 116–122.
[25] X. Chang, J. Huang, Q. Tan, M. Wang, G. Ji, S. Deng, G. Yu, Photocatalytic degradation of PCP-Na over BiOI nanosheets under simulated sunlight irradiation, Catal. Commun. 10 (2009) 1957–1961.
[26] Z. Baolong, C. Baishun, S. Keyu, H. Shangjin, L. Xiaodong, D. Zongjie, Y. Kelian, Preparation and characterization of nanocrystal grain TiO_2 porous microspheres, Appl. Catal. B-Environ. 40 (2003) 253–258.
[27] K. Hu, X. Xiao, X. Cao, R. Hao, X. Zuo, X. Zhang, J. Nan, Adsorptive separation and photocatalytic degradation of methylene blue dye on titanate nanotube powders prepared by hydrothermal process using metal Ti particles as a precursor, J. Hazard. Mater. 192 (2011) 514–520.
[28] J. Yu, W. Liu, H. Yu, A one-pot approach to hierarchically nanoporous titania hollow microspheres with high photocatalytic activity, Cryst. Growth Des. 8 (2008) 930–934.
[29] X. Xiao, W.D. Zhang, Facile synthesis of nanostructured BiOI microspheres with high visible light-induced photocatalytic activity, J. Mater. Chem. 20 (2010) 5866–5870.
[30] Y.Q. Lei, G.H. Wang, S.Y. Song, W.Q. Fan, M. Pang, J.K. Tang, H.J. Zhang, Room temperature, template-free synthesis of BiOI hierarchical structures: visible-light photocatalytic and electrochemical hydrogen storage properties, Dalton Trans. 39 (2010) 3273–3278.
[31] J. Xia, S. Yin, H. Li, H. Xu, Y. Yan, Q. Zhang, Self-assembly and enhanced photocatalytic properties of BiOI hollow microspheres via a reactable ionic liquid, Langmuir 27 (2010) 1200–1206.
[32] H. Xue, Z. Li, H. Dong, L. Wu, X. Wang, X. Fu, 3D hierarchical architectures of $Sr_2Sb_2O_7$: hydrothermal syntheses, formation mechanisms, and application in aqueous-phase photocatalysis, Cryst. Growth Des. 8 (2008) 4469–4475.
[33] L. Tian, H. Yao Tan, J.J. Vittal, Morphology-controlled synthesis of Bi_2S_3 nanomaterials via single- and multiple-source approaches, Cryst. Growth Des. 8 (2008) 734–738.
[34] J. Wang, Y. Xu, M. Hojamberdiev, M. Wang, G. Zhu, Polyvinylpyrrolidone (PVP)-assisted hydrothermal synthesis of luminescent YVO_4:Eu^{3+} microspheres, Mater. Chem. Phys. 119 (2010) 169–174.
[35] Y. Li, J. Liu, X. Huang, G. Li, Hydrothermal synthesis of Bi_2WO_6 uniform hierarchical microspheres, Cryst. Growth Des. 7 (2007) 1350–1355.
[36] K. Sing, D.H. Everett, R. Haul, L. Moscou, R.A. Pierotti, J. Rouquerol, T. Siemieniewska, IUPAC Recommendations 1984: reporting physisorption data for gas/solid systems with special reference to the determination of surface area and porosity, Pure Appl. Chem. 57 (1985) 603–619.

[37] J. Zhang, F. Shi, J. Lin, D. Chen, J. Gao, Z. Huang, X. Ding, C. Tang, Self-assembled 3-D architectures of BiOBr as a visible light-driven photocatalyst, Chem. Mater. 20 (2008) 2937–2941.
[38] L. Zhao, L. Gao, Coating multi-walled carbon nanotubes with zinc sulfide, J. Mater. Chem. 14 (2004) 1001–1004.
[39] L. Shen, N. Bao, Y. Zheng, A. Gupta, T. An, K. Yanagisawa, Hydrothermal splitting of titanate fibers to single-crystalline TiO_2 nanostructures with controllable crystalline phase, morphology, microstructure, and photocatalytic activity, J. Phys. Chem. C 112 (2008) 8809–8818.
[40] J. Li, H. Fan, J. Chen, L. Liu, Synthesis and characterization of poly(vinyl pyrrolidone)-capped bismuth nanospheres, Colloids Surf. A: Physiochem. Eng. Aspects 340 (2009) 66–69.
[41] J. Tang, Z. Zou, J. Ye, Efficient photocatalytic decomposition of organic contaminants over $CaBi_2O_4$ under visible light irradiation, Angew. Chem. Int. Ed. 43 (2004) 4463–4466.
[42] J. Xiong, G. Cheng, G. Li, F. Qin, R. Chen, Well-crystallized square-like 2D BiOCl nanoplates: mannitol-assisted hydrothermal synthesis and improved visible-light-driven photocatalytic performance, RSC Adv. 1 (2011) 1542–1553.
[43] F. Fang, L. Chen, L.M. Wu, Syntheses, morphologies and properties of BiOI nanolamellas and BiSI nanorods, Chin. J. Struct. Chem. 28 (2009) 1399–1406.
[44] H.Z. An, Y. Du, T.M. Wang, C. Wang, W.C. Hao, J.Y. Zhang, Photocatalytic properties of BiOX (X = Cl, Br, and I), Rare Metals 27 (2008) 243–250.
[45] X.F. Chang, J. Huang, Q.Y. Tan, M. Wang, G.B. Ji, S.B. Deng, G. Yu, Photocatalytic degradation of PCP-Na over BiOI nanosheets under simulated sunlight irradiation, Catal. Commun. 10 (2009) 1957–1961.
[46] J. Henle, P. Simon, A. Frenzel, S. Scholz, S. Kaskel, Nanosized BiOX (X = Cl, Br, I) particles synthesized in reverse microemulsions, Chem. Mater. 19 (2007) 366–373.
[47] W.R. Chen, C.H. Huang, Adsorption and transformation of tetracycline antibiotics with aluminum oxide, Chemosphere 79 (2010) 779–785.
[48] L.L. Ji, W. Chen, L. Duan, D.Q. Zhu, Mechanisms for strong adsorption of tetracycline to carbon nanotubes: a comparative study using activated carbon and graphite as adsorbents, Environ. Sci. Technol. 43 (2009) 2322–2327.
[49] P.H. Chang, Z.H. Li, T.L. Yu, S. Munkhbayer, T.H. Kuo, Y.C. Hung, J.S. Jean, K.H. Lin, Sorptive removal of tetracycline from water by palygorskite, J. Hazard. Mater. 165 (2009) 148–155.
[50] J. Kang, H. Liu, Y.M. Zheng, J. Qu, J.P. Chen, Application of nuclear magnetic resonance spectroscopy, Fourier transform infrared spectroscopy, UV–Visible spectroscopy and kinetic modeling for elucidation of adsorption chemistry in uptake of tetracycline by zeolite beta, J. Colloid Interface Sci. 354 (2010) 261–267.
[51] M.A. Gondal, X.F. Chang, Z.H. Yamani, UV-light induced photocatalytic decolorization of Rhodamine 6G molecules over BiOCl from aqueous solution, Chem. Eng. J. 165 (2010) 250–257.
[52] X. Chang, G. Ji, K. Shen, L. Pan, Y. Shi, Y. Zheng, Fabrication of nanowire-like cuprous oxide in aqueous solutions of a triblock copolymer, J. Alloys Compd. 482 (2009) 240–245.
[53] G. Zhang, J. Qu, H. Liu, A.T. Cooper, R. Wu, $CuFe_2O_4$/activated carbon composite: a novel magnetic adsorbent for the removal of acid orange II and catalytic regeneration, Chemosphere 68 (2007) 1058–1066.
[54] F. Haghseresht, G.Q. Lu, Adsorption characteristics of phenolic compounds onto coal-reject-derived adsorbents, Energy Fuels 12 (1998) 1100–1107.
[55] W. Chen, L. Duan, D. Zhu, Adsorption of polar and nonpolar organic chemicals to carbon nanotubes, Environ. Sci. Technol. 41 (2007) 8295–8300.
[56] Y. Yang, G. Zhang, S. Yu, X. Shen, Efficient removal of organic contaminants by a visible light driven photocatalyst $Sr_6Bi_2O_9$, Chem. Eng. J. 162 (2010) 171–177.
[57] Y.B. Liu, B.X. Zhou, J.H. Li, X.J. Gan, J. Bai, W.M. Cai, Preparation of short, robust and highly ordered TiO_2 nanotube arrays and their applications as electrode, Appl. Catal. B-Environ. 92 (2009) 326–332.
[58] P. Wang, P. Yap, T. Lim, C-N-S tridoped TiO_2 for photocatalytic degradation of tetracycline under visible-light irradiation, Appl. Catal. A: Gen. 399 (2011) 252–261.
[59] M.E. Lindsey, M. Meyer, E.M. Thurman, Analysis of trace levels of sulfonamide and tetracycline antimicrobials in groundwater and surface water using solid-phase extraction and liquid chromatography/mass spectrometry, Anal. Chem. 73 (2001) 4640–4646.